

# Experimental tests on scintillator tile light collection efficiency

M. Espirito-Santo, A. Gomes, A. Maio, L. Peralta, M. Pimenta, B. Tomé  
LIP-Lisbon

## Abstract

The measurement of light yield of plastic scintillating tiles, used in a "shashlik" type calorimeter is reported. The readout of these tiles is made by Wavelength Shifter fibers running perpendicularly to the tile. Measurements have also been made with tiles wrapped with a white diffuser paper. A Monte Carlo simulation of the light production and collection of these tiles has been developed. The simulated results are compared with the data.



# 1 Introduction

In recent years the so called "shashlik" [1] type of calorimeters has become very popular. These sampling calorimeters combine the compactness of standard sandwich sampling calorimeters and the true modularity achieved by spaghetti calorimeters [2]. In fact the standard sandwich calorimeters often had problems, concerning the way the light signal was readout from the scintillator tiles. Many of the solutions lead to dead spaces, damaging the modularity. This problem was overcome by the use of optical wavelength shift (WLS) fibers, that go across the scintillator tiles, and are readout in the back of the calorimeter.

The Small angle Tile Calorimeter (STIC) [3], the new DELPHI experiment luminosity monitor, is one of these calorimeters. The STIC is a low angle detector giving an angular coverage between 29 and 185 mrad. The calorimeter is divided in ten rings and 16 azimuthal sectors and it has a projective geometry towards the interaction point. Each scintillator plane has 160 individual tiles. The geometry of each tile is approximatively that of a cut circular sector. Each tile has a certain number of holes, for fibers passing through, and is totally wrapped in white Tyvek<sup>®</sup><sup>1</sup> paper. Thus each tile becomes in this way a complicated optical object. In order to know the tile efficiency for light collection, laboratory tests were performed and a Monte Carlo simulation was developed.

## 2 The laboratory tests

The aim of the laboratory tests was the measurement of the tiles response to ionizing particles. From that response the free parameters in the simulation could be extracted. Once these parameters are known, the tile collection efficiency maps can be computed [4].

### 2.1 The laboratory setup

In the laboratory tests the tiles were excited with  $\beta$  radiation emitted by a <sup>90</sup>Sr source. The <sup>90</sup>Sr source was sitting inside a plexiglas cylinder and 12 mm away from a 2 mm thick lead collimator with a 1 mm aperture (figure 1). The distance from the collimator to the tile was 5.5 mm. The plexiglas cylinder was fixed to a X-Y table, controlled by a computer and could be moved with 25  $\mu$ m steps. The scintillator tile was hold in place by a black plexiglas frame. The signal was taken out by green wavelength shifter fibers (Y7 Kuraray), the same as the ones used in the final detector. At the opposite side to tile, the fiber were hold by a clamp. The fibers end was 5 mm away from a light guide which was coupled to a XP2020 green extended photomultiplier. The tile, clamp and PM stood on a plexiglas grove allowing this elements to be positioned in a reproducible way. The whole setup was inside a light proof box.

### 2.2 System reproducibility

With this setup two kinds of reproducibility problems were faced. One was the placement of the radioactive source. For technical reasons the source had to be put away at the end of the day, and placed back into position, again, in the next day. The other question was

---

<sup>1</sup>Tyvek is Du Pont's registered trademark.

to verify that the standard precision of the X-Y table was indeed achieved when moving the radioactive source.

Two kinds of reproducibility tests were performed. In the first test the same scan was performed twice removing and putting back the source in between. The ratio of the result on these two scans are displayed in figure 2 where the deviations from unity are in the 5% range. In the second test the source was kept in place and the same scan was made twice. In figure 3 the result of two X scans and two Y are superimposed. The ratios of these scans also show variations bellow 5% .

## 2.3 The light collection maps

From the laboratory tests full light collection maps were obtained for chosen calorimeter tiles. Tests were made for naked tiles and for tiles wrapped in Tyvek<sup>®</sup> paper at lateral (thinner) tile faces. The full maps of the smaller tile, naked (a) and wrapped (b), are displayed in figure 4.

Systematic comparison between tiles, were obtained analyzing different map slices. Two kinds of bands were chosen: one cutting through the fibers (band B1) and one missing the fibers (band B2) (see figure 5). Six naked tiles were measured.

In figure 6 and figure 7 the average tile light output are shown respectively for band B1 and band B2. From these results some conclusions can be drawn. If the number of fibers is kept constant and the tile area increases, then the light output decreases. This feature seems quite trivial, since for a bigger tile the average length covered by a photon to be caught by a fiber is greater and so is the probability to get absorbed in the tile. However the light output increases from the tiles with 9 fibers to the tiles with 16 fibers although the number of fibers per  $\text{cm}^2$  does not increase (in fact it decreases). In this case a possible explanation may lay in the fact that for the bigger tiles, fibers are more uniformly distributed. For all tiles the measured average values for band B2 are lower than the values for band B1, since band B1 goes through the fibers.

The results for two wrapped tiles (a 9 hole and a 16 hole tile) are displayed in figure 8. An increase of the order of 50% in the light output was obtained, and the fiber peaks are smoothed out for both tiles.

## 2.4 Fibers direct response

Tests were made with the fibers on a black plexiglas board, to separate the direct contribution of the fibers to the signal output. The board had the shape of a 16 hole tile, so the fibers where exactly in the same positions as in the real tile. Measured values at the peak ranged from 10 to 14  $\mu\text{V}$ . Figure 9 shows a slice of a fibers scan. The direct response of the fibers give an important indication of the fibers light production efficiency, which is an important parameter that will be discussed bellow.

# 3 The Monte Carlo Simulation

The main objective of the Monte Carlo program was to find, for each point on the tile, the probability of a photon produced there to be collected by the WLS fibers. The amount (probability) of light leaking from the tile surfaces was also computed. The program has

three free parameters: the effective light attenuation in the tile  $\lambda_{at}$  (as defined in 3.3), the effective diffuser paper reflectivity ( $R$ ) and the fibers relative light production efficiency  $r_{fib}$  (as defined in 4.1).

The program flow is sketched in figure 10. A point at the scintillator is chosen to emit light. The way this is done depends on the type of simulation. The point might be chosen in a uniform random way all over the tile volume or according to some volume distribution. At the each new generated point  $(x, y, z)$  a new direction of light emission is also generated in an isotropic way. A check is made to see if the  $(x, y, z)$  point is inside the scintillator. A tracing routine is then called. Between two interfaces the light is assumed to travel in a straight line (no dispersion inside the tile). At the interface the light is reflected or transmitted (according to Snell's law). In the case of the interface between the scintillator (or a fiber) and air a specular reflection is assumed, and the reflection coefficient is computed with the Fresnel relations [5], [6] assuming non-polarized light. If the interface is between air and white paper the reflection is performed according to an isotropic diffusion. Between two consecutive reflections (or transmission), light can be absorbed in the medium. Different media have different light attenuation coefficients. The program stops following a photon when he is absorbed in the medium or he is lost through the walls.

### 3.1 The light generation

The simulation of the laboratory test conditions and of the production of light collection maps involved two different light generation algorithms, as the tile was excited in the laboratory by a  $^{90}\text{Sr}$   $\beta$  source.

For production of light collection efficiency maps, the light is generated in an uniform random way all over the tile volume.

For the simulation of the laboratory tests conditions the amount of light produced at a certain point is proportional to the  $\beta$  particle deposited energy at that point.

The interaction of the  $\beta$  particles with the scintillator was simulated using the EGS4 code [7]. The energy spectrum of an electron emitted by a  $\beta$  source of atomic number  $Z$ , can be parameterized as [8]

$$dN = C \cdot F(Z, E_k) (E_k - E_o)^2 p^2 dp$$

where  $E_k$ ,  $E_o$  and  $p$  are respectively the kinetic and the maximum kinetic energy and momentum of the beta particle.  $F(Z, E_k)$  is the Fermi function [9], which corrects for the Coulomb distortion of the electron wave function [10]. The factor  $C$ , which includes the transition matrix element, can in first order be regarded as constant [8].

The lateral and longitudinal profiles for energy deposition by the  $\beta$  particles obtained in this way are displayed in figure 11. At each tile surface point these profiles define the source spot.

### 3.2 The tracking inside a tile

In this routine it was assumed that each photon travels in a straight line, between two walls (i.e. the borders between two media). This approximation neglects the diffusion effects in the medium.

The walls are defined by simple geometrical elements, such as planes, cylinders etc. To find the next interface point where the photon will hit, the program just had to find all the intersections points between these walls and the straight line defined by the actual point where the photon was and by its propagation direction. The next intersection point will be the nearest one in the propagation direction.

### 3.3 The photon absorption

The photon, on its path between two interfaces, might be absorbed in the medium. Following the well known relation for the attenuation of a monochromatic light beam  $I(x) = I_o \exp(-x/\lambda_{at})$ , where  $I(x)$  is the beam intensity after a length  $x$ ,  $I_o$  the initial intensity, and  $\lambda_{at}$  the light attenuation coefficient, the probability for a photon absorption on a path of length  $X$  is given by

$$1 - I(X)/I_o = 1 - \exp(-X/\lambda_{at})$$

In general the light attenuation coefficient depends on the light wavelength, but in a first order approximation an effective value is taken. In a second approximation two or more different light attenuation were considered.

In the scintillator tile the light attenuation values are in the range of 40 to 10 cm. The effective attenuation value is a parameter extracted from the comparison of laboratory tests and the simulation.

The light produced by the tile is absorbed and wavelength shifted by the fibers. In what concerns this simulation, a photon is captured when it is absorbed in a fiber. The attenuation length for the tile light in the fiber is very small. A value of the order of  $250\mu\text{m}$  was found to be compatible with the tests made in laboratory.

### 3.4 Reflection and refraction of the light

The reflection and refraction on the tile walls were made according to Snell's law [5] (appendix A). The probabilities of reflection and refraction on the tile walls were taken from Fresnel relations (appendix B).

The reflection on paper was done using an isotropic diffusing surface. An effective reflection coefficient  $R$  was assigned to the paper. This value is lower than the real one, and takes into account effects not fully described by the Monte Carlo (like light escaping through "holes"). As  $R < 1$  there is a probability for the photon to be "absorbed" in the paper. In general this means that the probability for absorption in the paper plus transmission through the paper is  $1 - R$ . The parameter  $R$  was extracted by comparison between the simulation and the laboratory tests.

### 3.5 The light production and collection in the fibers

The light generation inside the fiber took into account the relative light yield between the fiber and the scintillator tile. A 100% collection probability was assumed for the photons produced inside the fiber.

## 4 Data comparison with Monte Carlo

### 4.1 The method

From the comparison between laboratory test data and Monte Carlo simulation the free parameters of the simulation were extracted. These parameters are:  $\lambda_{at}$  the effective light attenuation length in the tile,  $r_{fib}$  the ratio between the light production in the fibers and the light production in the tile, and  $R$  the effective reflection coefficient of the Tyvek® paper. The first two parameters, were found with the naked tiles measurements. The tests with wrapped tiles provided the  $R$  parameter. To begin the comparison between the Monte Carlo and the data, values of  $\lambda_{at}$  and  $r_{fib}$  were chosen.

The values of  $\lambda_{at}$  were measured by the tile manufacturer and the values are in the range of 20 to 40 cm.

The value of  $r_{fib}$  must be low (the fibers in STIC are WLS) but as it was discussed in paragraph 2.4 it is not zero. A crude estimation of  $r_{fib}$  was obtained by dividing the direct response of the fibers ( $y_{fib}$ ) as obtained in paragraph 2.4 by the measured light output in a point in the tile far from the fibers  $y_{tile}$ , corrected for the collection efficiency ( $\epsilon_{coll}$ )

$$r_{fib} \approx \frac{y_{fib}}{y_{tile}/\epsilon_{coll}}$$

$\epsilon_{coll}$  was estimated by the simulation described in chapter 3. The  $r_{fib}$  value ranges from 0.1 to 0.3 depending on which tile the fibers are inserted in.

For each tile and band the quality of the adjustment between the simulation and the measurements was quantified by a  $\chi^2$  value defined as

$$\chi^2 = \frac{1}{N} \sum_{i=1}^N \frac{(f_{data}(x_i) - f_{sim}(x_i))^2}{\sigma^2}$$

where  $f_{data}$  and  $f_{sim}$  are respectively the light output measured at the position ( $x_i$ ) and the simulated value,  $N$  is the number of data points and  $\sigma$  is the experimental error (which is taken to be 5%). Since the simulation gives a light collection efficiency for the tile, and the experimental measured light output is given in  $\mu\text{V}$  there exists an overall normalization factor between them. This parameter is called the  $K$  factor so that  $f_{sim}(x_i) = K \cdot e_{sim}(x_i)$ , where  $e_{sim}(x_i)$  is the Monte Carlo light collection efficiency for the  $x_i$  point. If light production in the tiles did not change from tile to tile then, the  $K$  factor would be a constant. In fact  $K$  was considered as an additional parameter and a minimum dispersion between different tiles was required.

The global simulation strategy was to simulate tile maps for different  $\lambda_{at}$  and  $r_{fib}$ , and calculate the  $\chi^2(K)$  distributions for each generated map. The combination of  $\lambda_{at}$  and  $r_{fib}$  which minimize both dispersion and the absolute value of  $\chi^2$  curves for all tiles was selected.

The performance of the method was tested using Monte Carlo data. A reference sample with  $\lambda_{at} = 20$  cm and  $r_{fib} = 0.1$  was simulated and compared with samples with different values of  $\lambda_{at}$  and  $r_{fib}$ . In figure 12 is presented the results obtained with the bands B2 for the  $\chi^2(K)$  plots of the values  $\lambda_{at} = 5, 10, 20, 30, 40$  cm and  $r_{fib} = 0.1$ . The curves of  $\chi^2(K)$  superimposes only when the correct value of  $\lambda_{at}$  is chosen.

## 4.2 Extracting the MC parameters

The extraction of the free parameters was made in successive steps selecting situations where a reasonable independence between the parameters was verified.

The parameter extraction started by simulating the tile response in the band "in between the fibers" (band B2) where the influence of the parameter  $r_{fib}$  should be small. In this way the most important parameter to fit in this band was the effective light attenuation coefficient  $\lambda_{at}$ . In these simulations the  $r_{fib}$  value was fixed at 0.1. For each of the 6 naked tiles the light collection efficiency in band B2 was simulated for the light attenuation values  $\lambda_{at} = 5, 10, 15, 20, 40$  cm. The results are summarized in figures 13 where the normalization factor  $K$  and the  $\chi^2$  are plotted against  $\lambda_{at}$ . These plots favoured the values  $\lambda_{at} = 10$  and 15 cm.

The extraction of  $r_{fib}$  was made using band the B1, that goes through the fibers. The tile bands were simulated with  $\lambda_{at} = 10$  and 15 cm and  $r_{fib} = 0.05, 0.1$  and 0.15. The results are presented in figures 14. The compromise between minimal dispersion and minimal  $\chi^2$  values points of  $r_{fib} = 0.1$ .

Finally the analysis of the Tyvek<sup>®</sup> wrapped tiles data allows the extraction of the  $R$  parameter and to select the best value for  $\lambda_{at}$ . The comparison between the experimental data and the simulation for different effective paper reflection coefficient are made in figures 15, for  $\lambda_{at} = 15$  cm and  $r_{fib} = 0.1$ . The best agreement is achieved when  $R$  is set to 0.6. The results for small and big tiles cannot be reproduced by setting  $\lambda_{at} = 10$  cm and using the same  $R$  value (figure 16). The free parameters of the simulation were therefore set to  $\lambda_{at} = 15$  cm,  $r_{fib} = 0.1$  and  $R = 0.6$ .

## 5 Conclusions

The measurement of the light yield of plastic scintillating tiles, used in a "shashlik" type calorimeter was made. The readout of this tiles were made by Wavelength Shifter fibers (Y7 Kuraray) running perpendicularly to the tile. Full scans of different size tiles were performed. The results concerning two chosen bands have been presented and compared with a Monte Carlo simulation. Three simulation parameters have been tuned by comparing data and Monte Carlo: the effective light attenuation in the tile  $\lambda_{at}$ , the effective diffuser paper reflectivity ( $R$ ) and the fibers relative light production efficiency  $r_{fib}$ .

Using the Monte Carlo simulation for the tile light collection efficiency and the parameters  $\lambda_{at}$ ,  $r_{fib}$  and  $R$ , efficiency light collection maps were produced [4]. These maps have been integrated in the full STIC calorimeter simulation [11], [12], which allows the description of the data at the per mill level.

## Acknowledgement

We are greatly indebted to our technical staff, J. Patriarca and M. Stielau for their assistance in the laboratory.

## Appendix A: Reflection and refraction between two dielectric media

Let  $\vec{n}$  be the unitary vector normal to the interface between the two media at the incident point, and  $\vec{i}$ ,  $\vec{r}$ ,  $\vec{t}$  the unitary vectors of the incident, reflected and transmitted rays (figure 17).

The vectors  $\vec{r}$  and  $\vec{t}$  can be determined as a function of  $\vec{n}$  and  $\vec{i}$ , with the angles  $\theta_i$  and  $\theta_t$ . Since  $\vec{r}$  and  $\vec{t}$  are in the same plane of  $\vec{n}$  and  $\vec{i}$ , they can be written as a linear combination of  $\vec{n}$  and  $\vec{i}$

$$\vec{r} = a_1 \vec{i} + a_2 \vec{n}$$

$$\vec{t} = b_1 \vec{i} + b_2 \vec{n}$$

To evaluate the constants  $a_1, a_2, b_1$  and  $b_2$  the internal products of  $\vec{r}$  and  $\vec{t}$  with  $\vec{i}$  and  $\vec{n}$  are computed.

$$\vec{r} \cdot \vec{i} = \cos(\pi - (\theta_i + \theta_r)) = -\cos 2\theta_i$$

$$\vec{r} \cdot \vec{n} = \cos(\pi - \theta_r) = -\cos \theta_r$$

but

$$\vec{r} \cdot \vec{i} = a_1 \vec{i} \cdot \vec{i} + a_2 \vec{n} \cdot \vec{i} = a_1 + a_2 \cos \theta_i$$

$$\vec{r} \cdot \vec{n} = a_1 \vec{i} \cdot \vec{n} + a_2 \vec{n} \cdot \vec{n} = a_1 \cos \theta_i + a_2.$$

resulting in the set of equations

$$-\cos 2\theta_i = a_1 + a_2 \cos \theta_i$$

$$-\cos \theta_i = a_1 \cos \theta_i + a_2$$

which have the solution

$$a_1 = 1 \quad \text{and} \quad a_2 = -2 \cos \theta_i.$$

The coefficients  $b_1, b_2$  are obtained in a similar way

$$\vec{t} \cdot \vec{i} = \cos(\theta_t - \theta_i) = b_1 + b_2 \cos \theta_i$$

$$\vec{t} \cdot \vec{n} = \cos \theta_t = b_1 \cos \theta_i + b_2$$

The solutions are

$$b_1 = \frac{\sin \theta_t}{\sin \theta_i} \quad \text{and} \quad b_2 = \frac{\sin(\theta_i - \theta_t)}{\sin \theta_i}$$

or using the Snell's law  $n_i \sin \theta_i = n_t \sin \theta_t$ ,  $b_1 = n_i/n_t$ . The complete solution is

$$\vec{r} = \vec{i} - 2 \cos \theta_i \vec{n}$$

$$\vec{t} = \frac{n_i}{n_t} \vec{i} + \frac{\sin(\theta_i - \theta_t)}{\sin \theta_i} \vec{n}$$

If  $n_i > n_t$  then there is only a transmitted ray whenever the incidence angle  $\theta_i$  is less than the critical angle  $\theta_c$  given by

$$\theta_c = \arcsin \frac{n_t}{n_i}.$$

## Appendix B: The Fresnel relations

The Fresnel relations for the reflection and transmission coefficients can be written as [6]

$$r_{\perp} = \left( \frac{E_0^r}{E_0^i} \right)_{\perp} = -\frac{\sin(\theta_i - \theta_t)}{\sin(\theta_i + \theta_t)}$$

$$r_{\parallel} = \left( \frac{E_0^r}{E_0^i} \right)_{\parallel} = \frac{\tan(\theta_i - \theta_t)}{\tan(\theta_i + \theta_t)}$$

$$t_{\perp} = \left( \frac{E_0^t}{E_0^i} \right)_{\perp} = \frac{2 \sin \theta_t \cos \theta_i}{\sin(\theta_i + \theta_t)}$$

$$t_{\parallel} = \left( \frac{E_0^t}{E_0^i} \right)_{\parallel} = \frac{2 \sin \theta_t \cos \theta_i}{\sin(\theta_i + \theta_t) \cos(\theta_i - \theta_t)}$$

The reflectivity  $R$  and transmissivity  $T$  defined respectively as the ratio between the incident amount of energy on a unit area per second to the reflected and transmitted ones, are given by [5]

$$R = \left( \frac{E_0^r}{E_0^i} \right)^2$$

$$T = \left( \frac{E_0^t}{E_0^i} \right)^2 \frac{n_t \cos \theta_t}{n_i \cos \theta_i}$$

The energy conservation implies that  $R + T = 1$ . It can be assigned to  $R$  and  $T$  the meaning of the probability to a ray to be reflected or transmitted.

For the parallel and transversal components of the electromagnetic wave a reflectivity and transmissivity are also define in a similar way [5] Again the relations  $R_{\perp} + T_{\perp} = 1$  and  $R_{\parallel} + T_{\parallel} = 1$  are verified.

Now let  $\alpha$  be the angle between the incident electromagnetic field vector  $\vec{E}_i$  and the plane of incidence. The parallel and transverse components of the field  $\vec{E}_i$  can be written as

$$(E_0^i)_{\perp} = E_0^i \sin \alpha \text{ and } (E_0^i)_{\parallel} = E_0^i \cos \alpha$$

The reflectivity  $R$  is then expressed in terms of  $R_{\perp}$  and  $R_{\parallel}$  as

$$R = R_{\perp} \cos^2 \alpha + R_{\parallel} \sin^2 \alpha$$

Assuming the light is not polarized, an average over  $\alpha$  must be made in order to get the reflectivity

$$\overline{R} = \frac{1}{2\pi} \int_0^{2\pi} R d\alpha$$

leading to

$$\overline{R} = \frac{1}{2}(R_{\perp} + R_{\parallel}) = \frac{1}{2}(r_{\perp}^2 + r_{\parallel}^2)$$

In the case of normal incidence  $\theta_i = 0$  and

$$\overline{R} = R = R_{\perp} = R_{\parallel} = \left( \frac{n_t - n_i}{n_t + n_i} \right)^2$$

## References

- [1] G. Atojan et al., *Nuc. Instr. Meth.* A320 (1992) 144
- [2] M. Livan, V. Vercesi and R. Wigmans, "Scintillating-fibre calorimetry", CERN 95-02
- [3] T. Camporesi et al., "The DELPHI Small Angle Tile Calorimeter", presented at the Beijing Calorimeter Conference, Beijing, 1994.
- [4] M. Espirito-Santo, "Um estudo do Calorímetro STIC para DELPHI, Master Thesis, University of Lisbon, 1995, unpublished.
- [5] M. Born and E. Wolf, "Principles of Optics", 1980 6th ed., Pergamon Press
- [6] E. Hecht, "Optics", 1987, 2nd ed., Addison-Wesley Publishing Company
- [7] W.R. Nelson, H. Hirayama, D. W.O. Rogers, "The EGS4 Code System", SLAC-Report-265, December 1985
- [8] K.S. Krane, "Introductory Nuclear Physics", 1988, John Wiley and Sons, New York
- [9] M. Morita, "Beta Decay and Muon Capture", Benjamin, Reading, Massachusetts, 1973.
- [10] S.S.M. Wong, "Introductory Nuclear Physics", Prentice-Hall, 1990
- [11] M. Espirito-Santo et al, "Fast Simulation of an Electromagnetic Calorimeter: a two stage approach", LIP/ 95-09, (1995), unpublished
- [12] M. Bonesini, S. Gumenyuk, M. Paganoni, L. Petrovykh, M. Bigi, E. Vallazza, G. Della Ricca, "Simulation of the DELPHI STIC calorimeter", DELPHI note 93-118 CAL 106, 1993

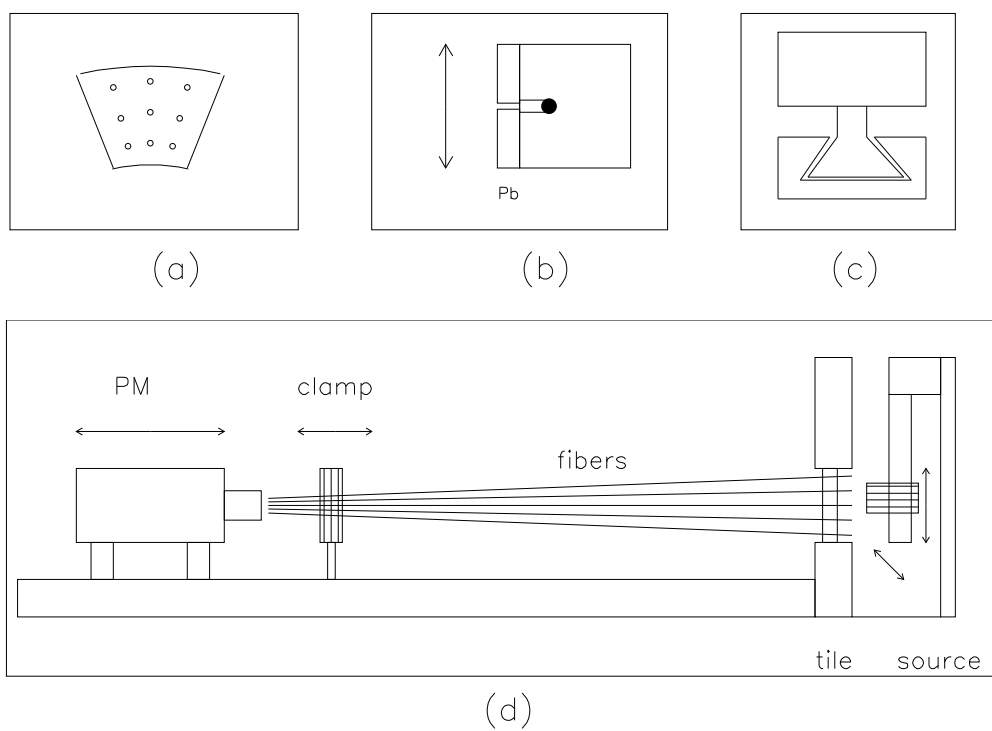


Figure 1: The laboratory setup. a) A small tile. b) The  $^{90}\text{Sr}$  source box and collimator. c) Table frontal view. d) The full setup.

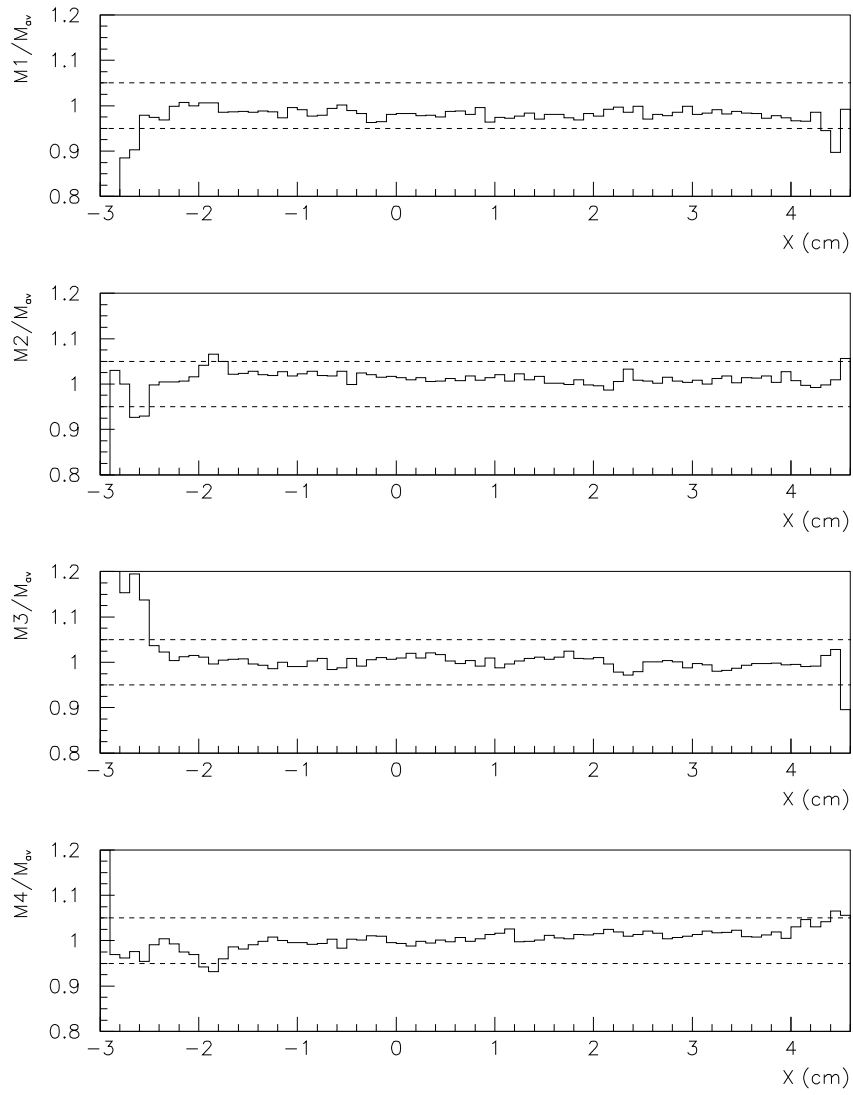


Figure 2: Reproducibility plots: for each scan the source was removed and put back again into position. From these scans an average scan profile was computed. The ratio between the average scan and the individual ones is displayed.

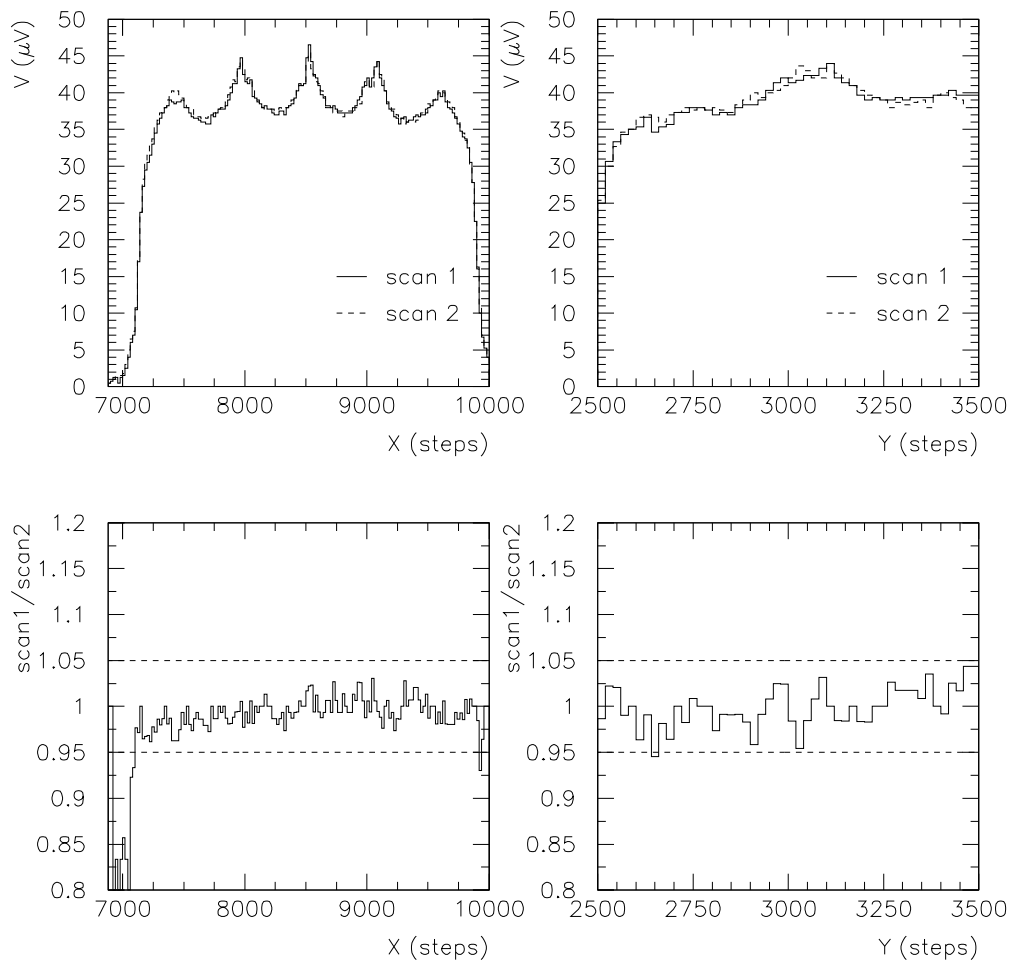


Figure 3: Top) Two x scans (left) and two y scans (right) of the same tile are superimposed. The light yield (vertical scale) is expressed in  $\mu\text{V}$  Bottom) Ratio of the two x and y scans.

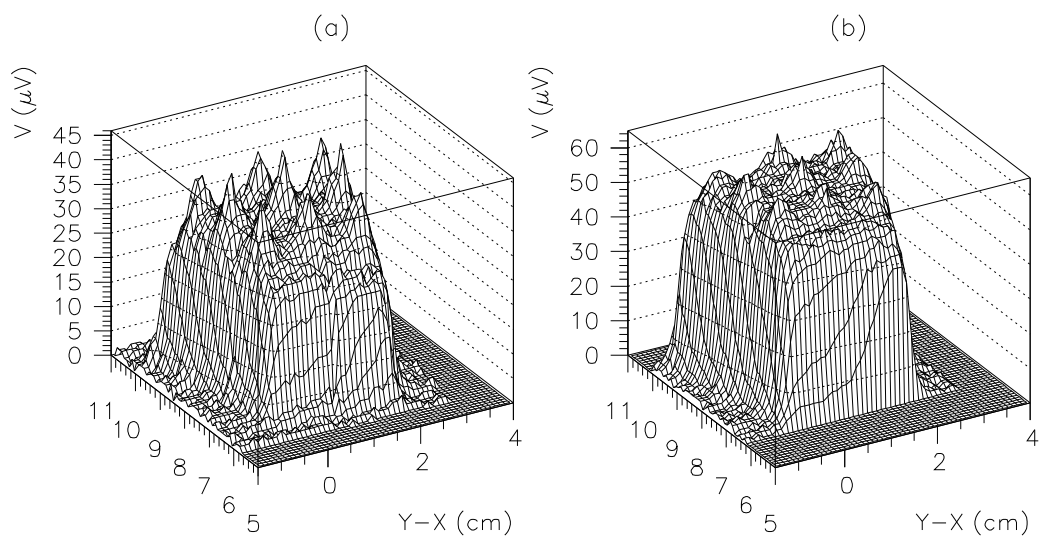


Figure 4: A xy full map scan. a) A "naked" tile b) A tile wrapped with Tyvek on the lateral surfaces. The light yield is expressed in  $\mu\text{V}$ .

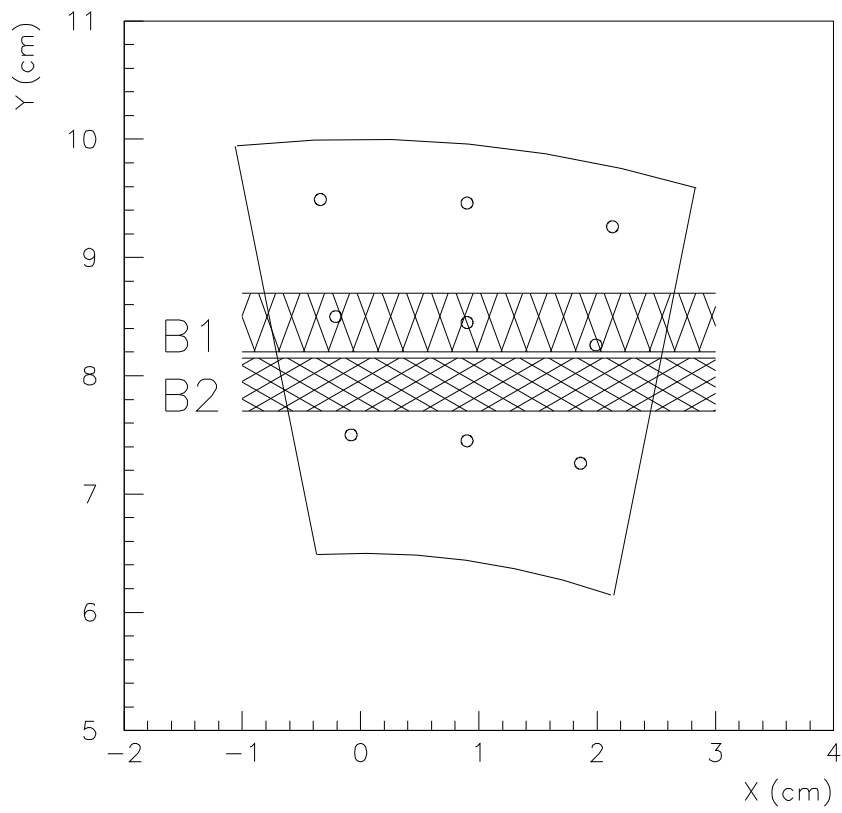


Figure 5: The top shaded area defines the B1 band (that goes through the fibers) and the bottom shaded area defines band B2.

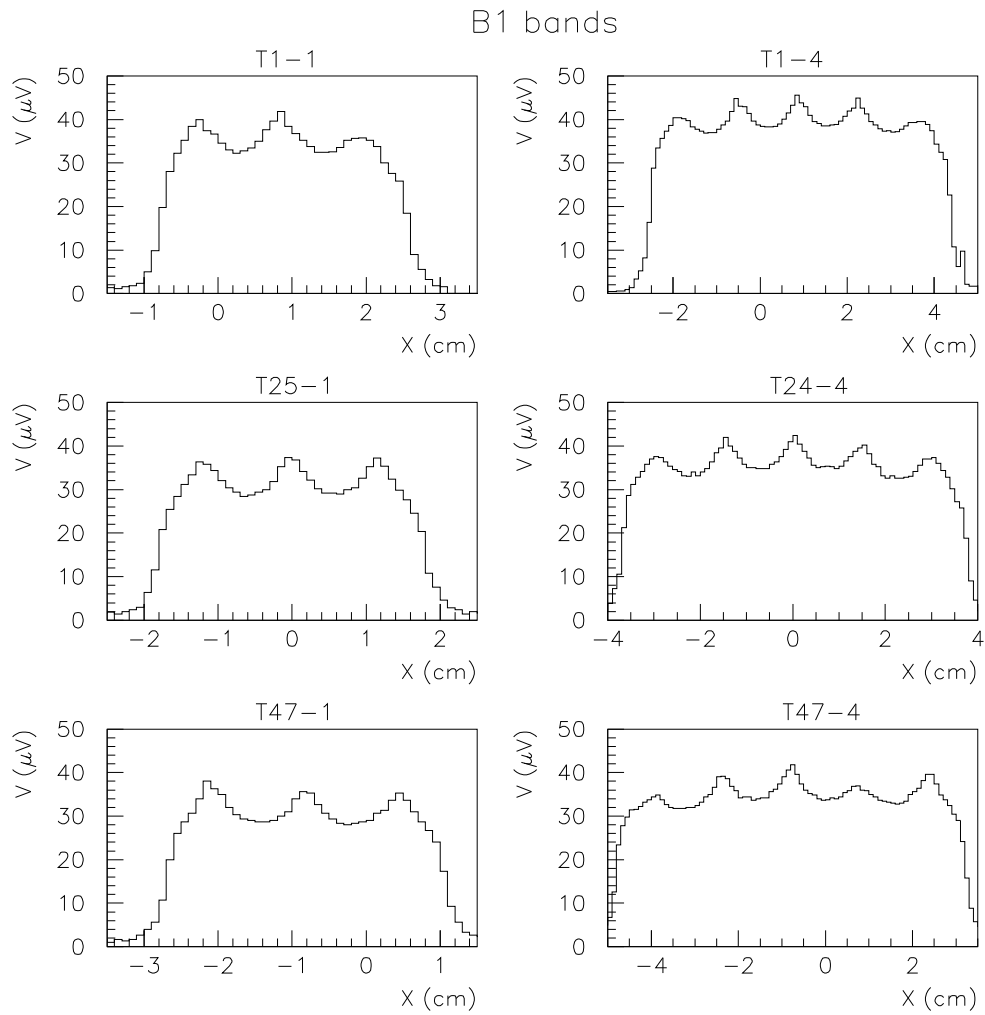


Figure 6: Scan results on band B1 for different naked tiles. The tile numbering give the longitudinal (plane number) and radial (ring number) position of the tiles in the calorimeter.

B2 bands

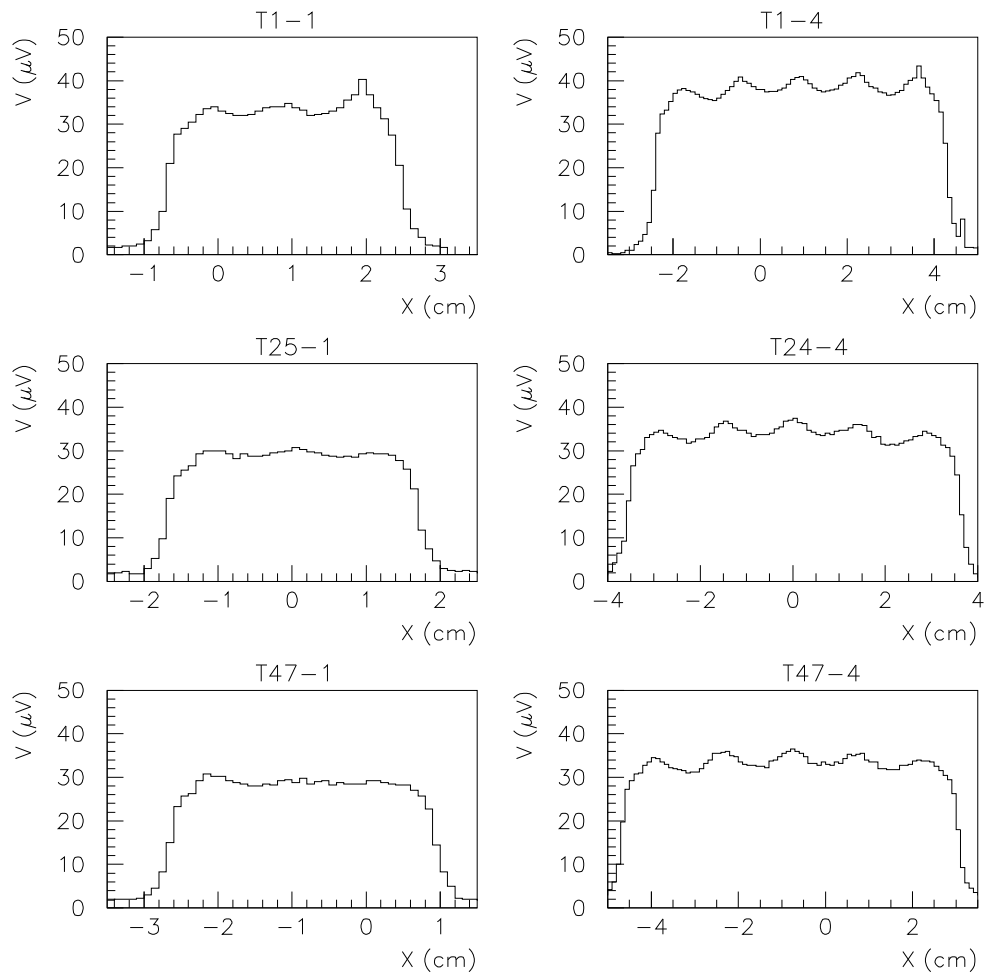


Figure 7: Scan results on band B2 for different naked tiles.

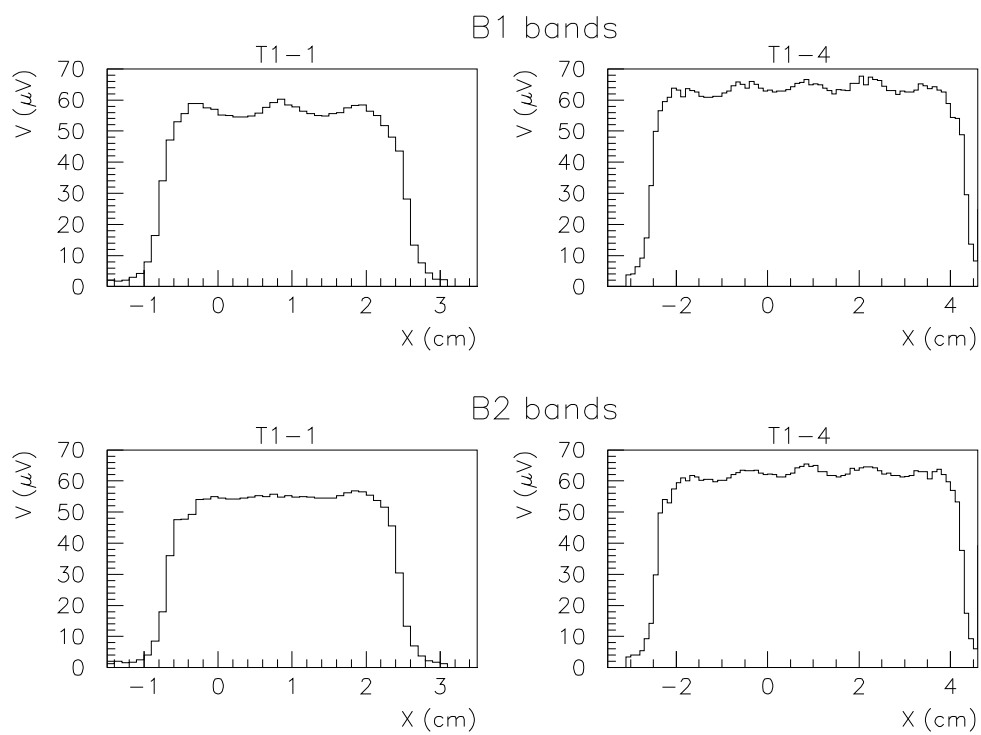


Figure 8: Scan results on bands B1 and B2 for two tiles wrapped with Tyvek on the lateral surfaces.

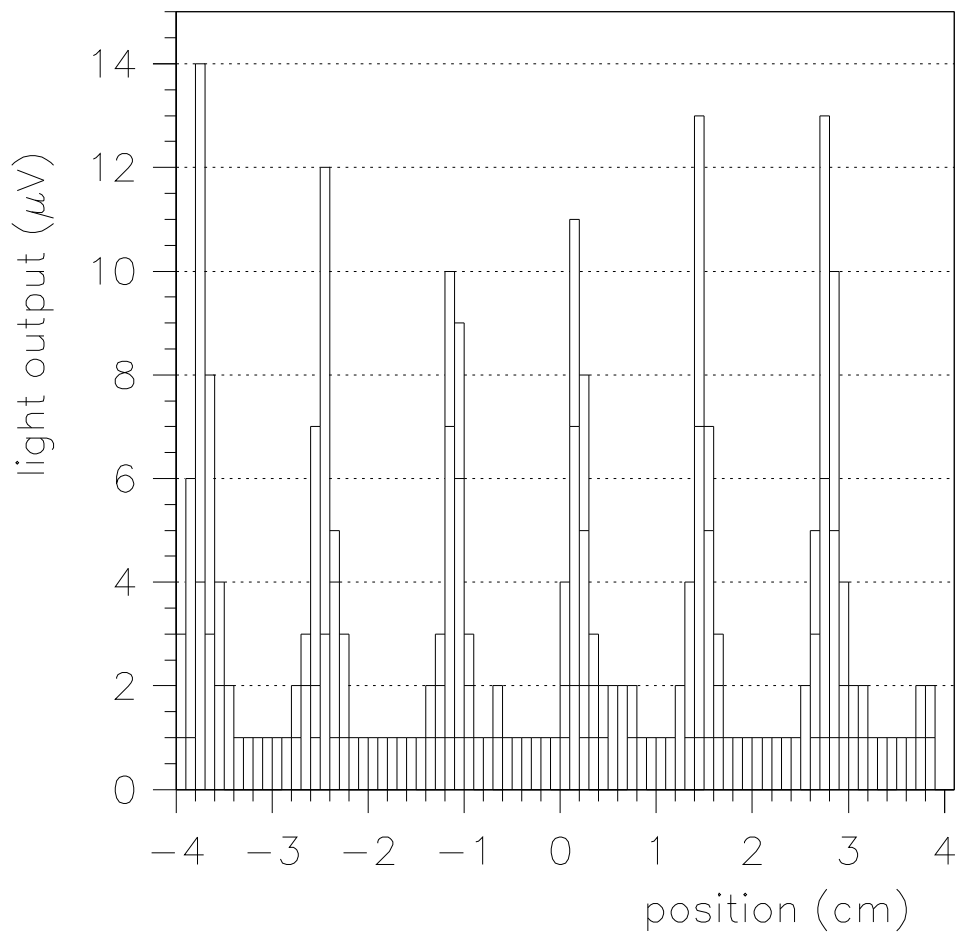


Figure 9: Light output of WLS fibers placed at a black tile.

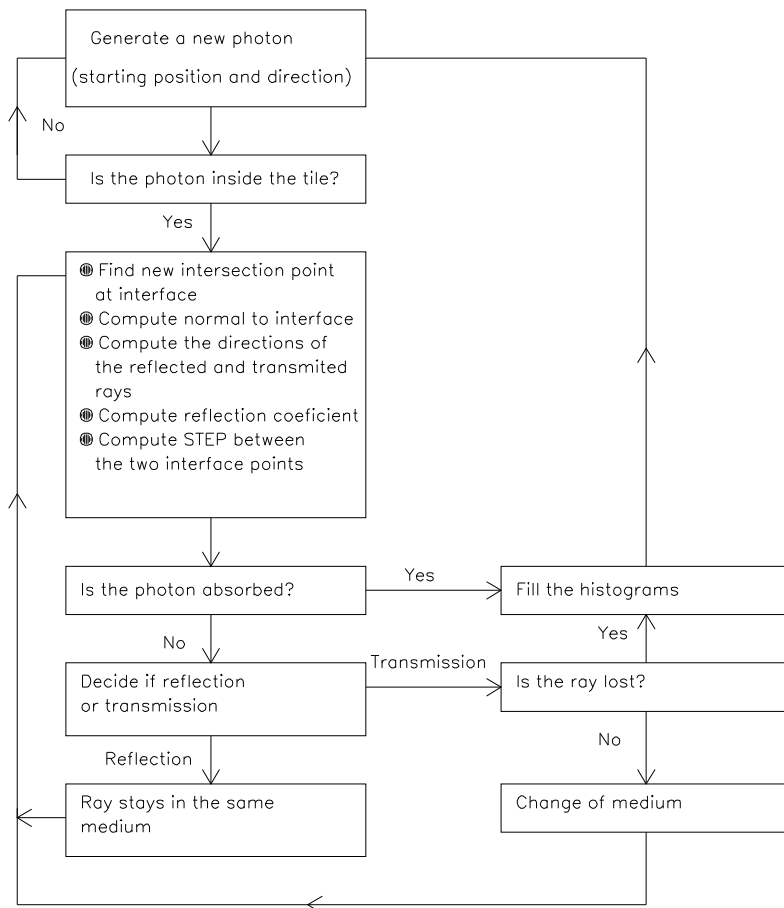


Figure 10: Program flow.

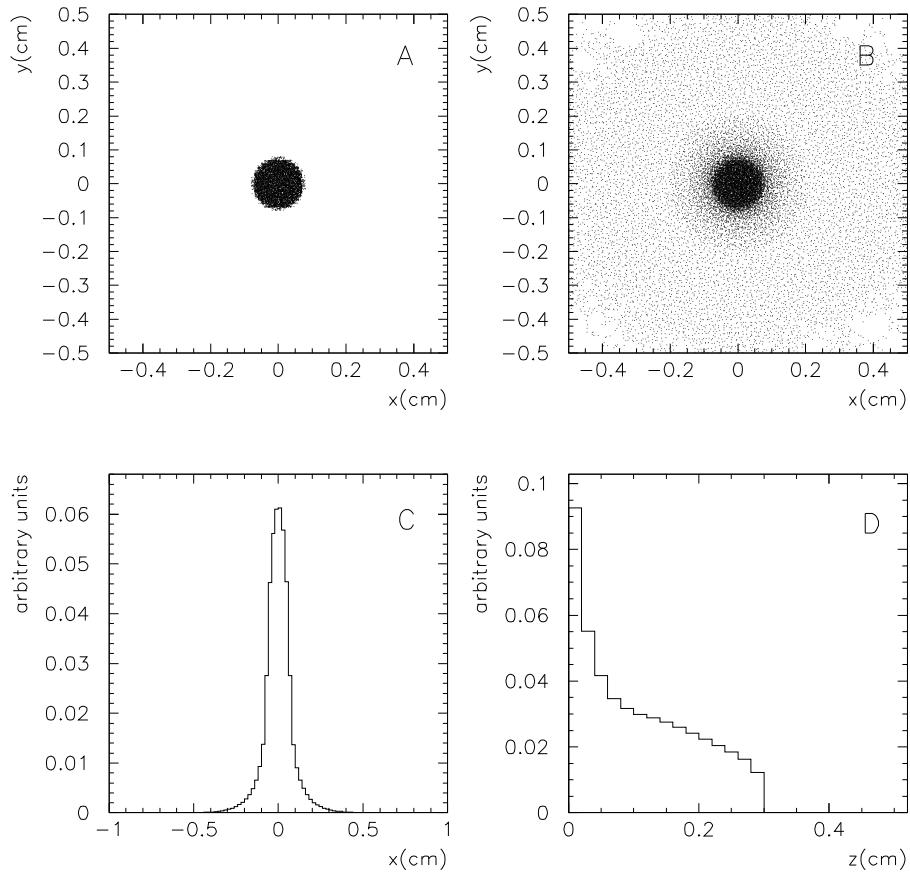


Figure 11: Energy deposition of the electrons emitted by the  $^{90}\text{Sr}$  source on a 3 mm thick tile. A) x-y source spot at the tile's entrance surface. B) x-y distribution of the electron energy deposition inside the tile. C) x profile of the energy deposition distribution inside the tile. D) Longitudinal profile of the energy deposition distribution inside the tile.

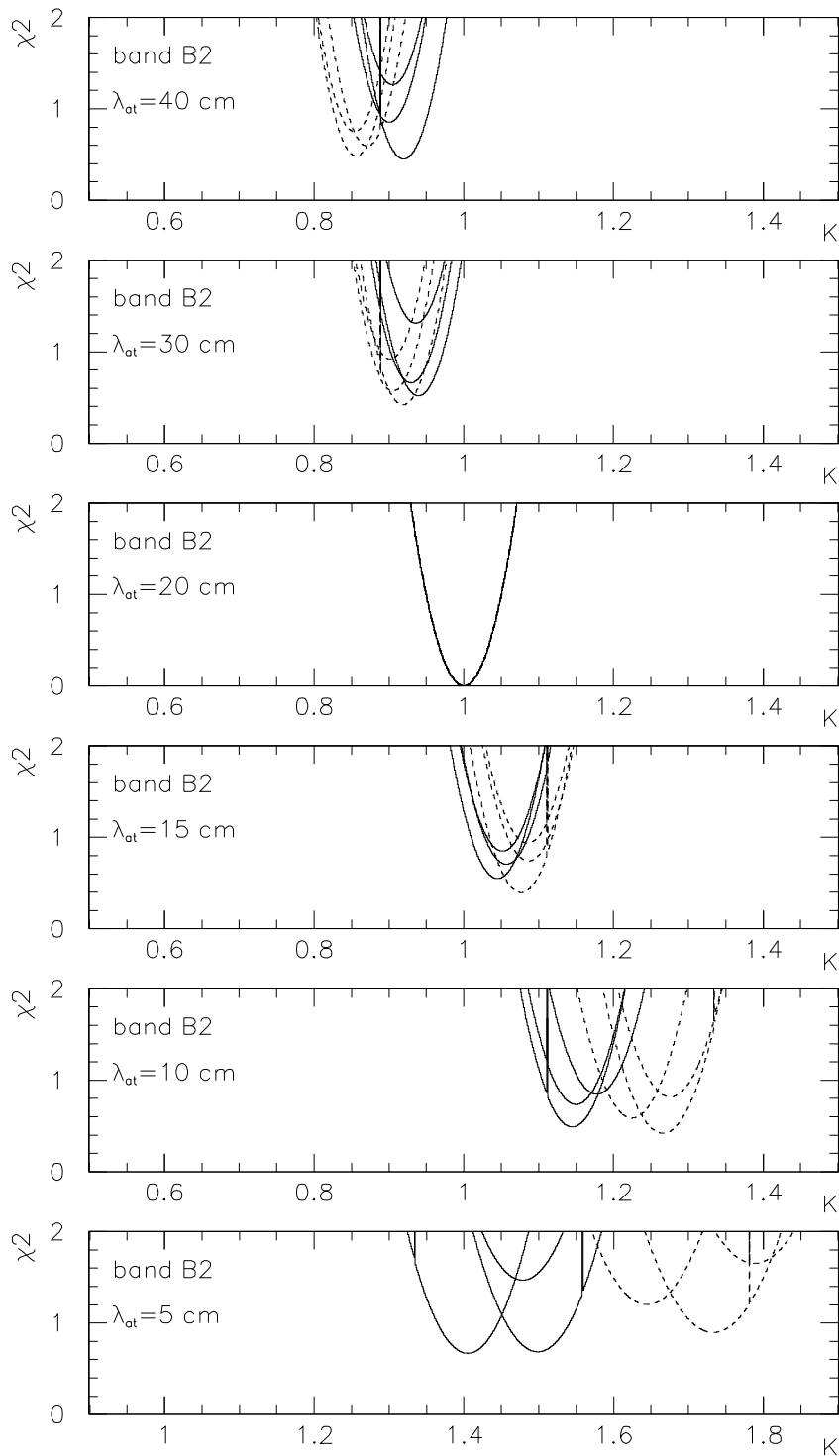


Figure 12: Simulation of the  $\chi^2$  behaviour as a function of the global normalization factor  $K$  for different  $\lambda_{at}$  values. The true (at the simulation) value for  $\lambda_{at}$  is 20 cm.

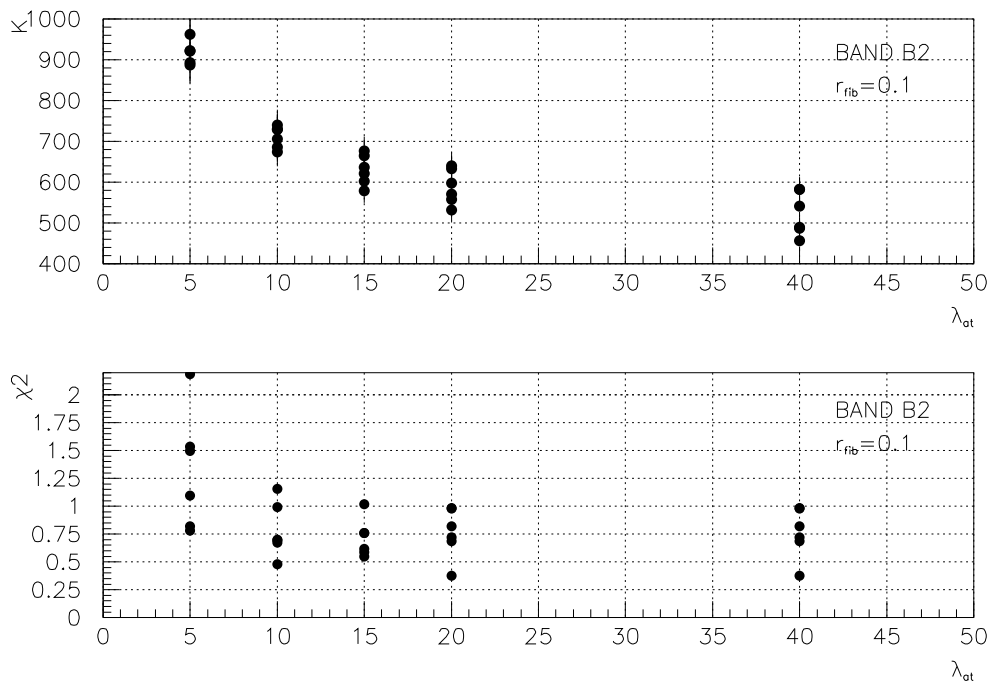


Figure 13:  $K$  and  $\chi^2$  (best values) for band B2 scans as a function of the simulated  $\lambda_{at}$  for the tiles.

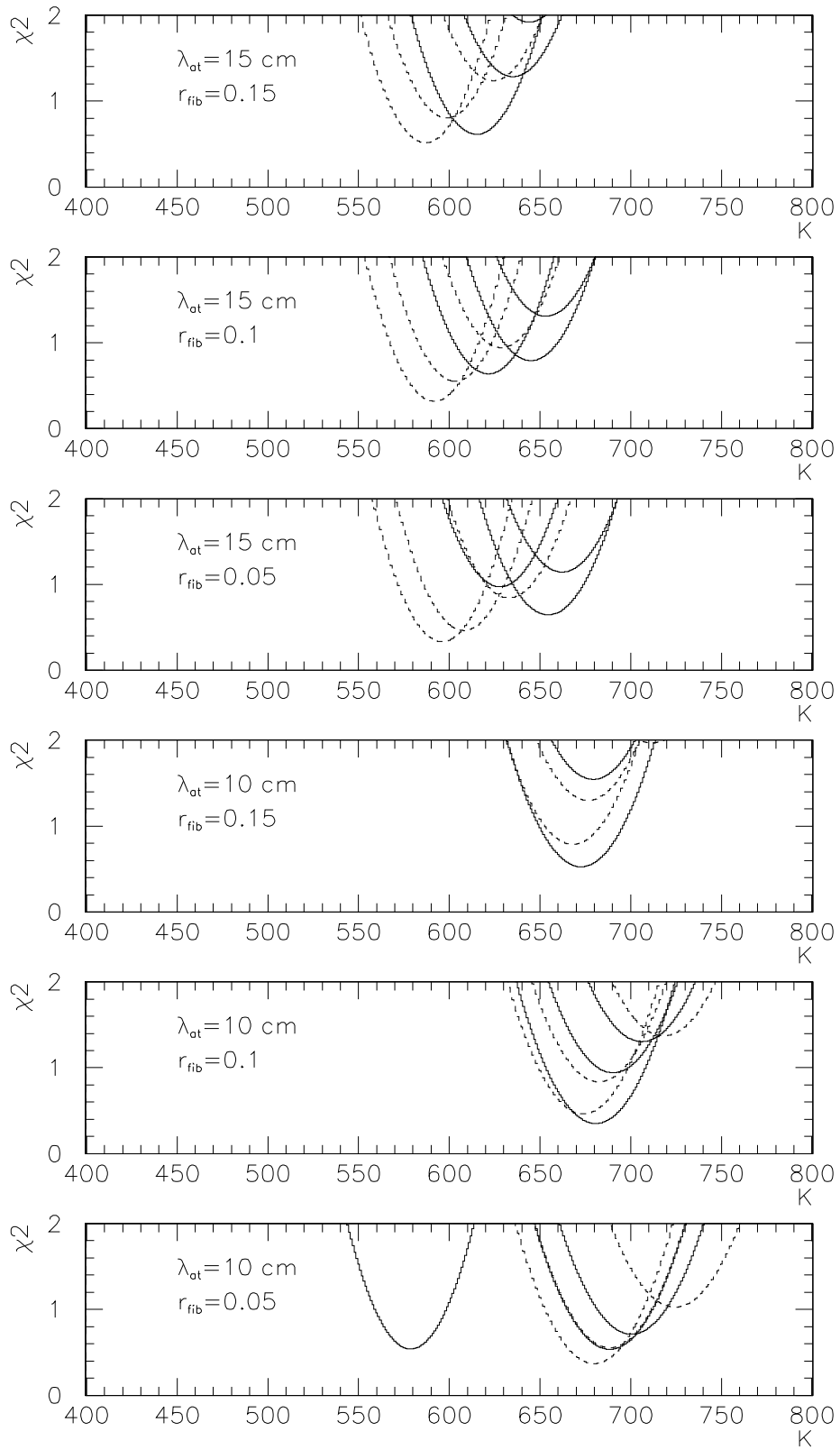


Figure 14:  $\chi^2$  values as a function of  $K$  for simulated  $\lambda_{at} = 15$  and 10 cm and  $r_{fib} = 0.05$ , 0.1 and 0.15 for B1 band scans.

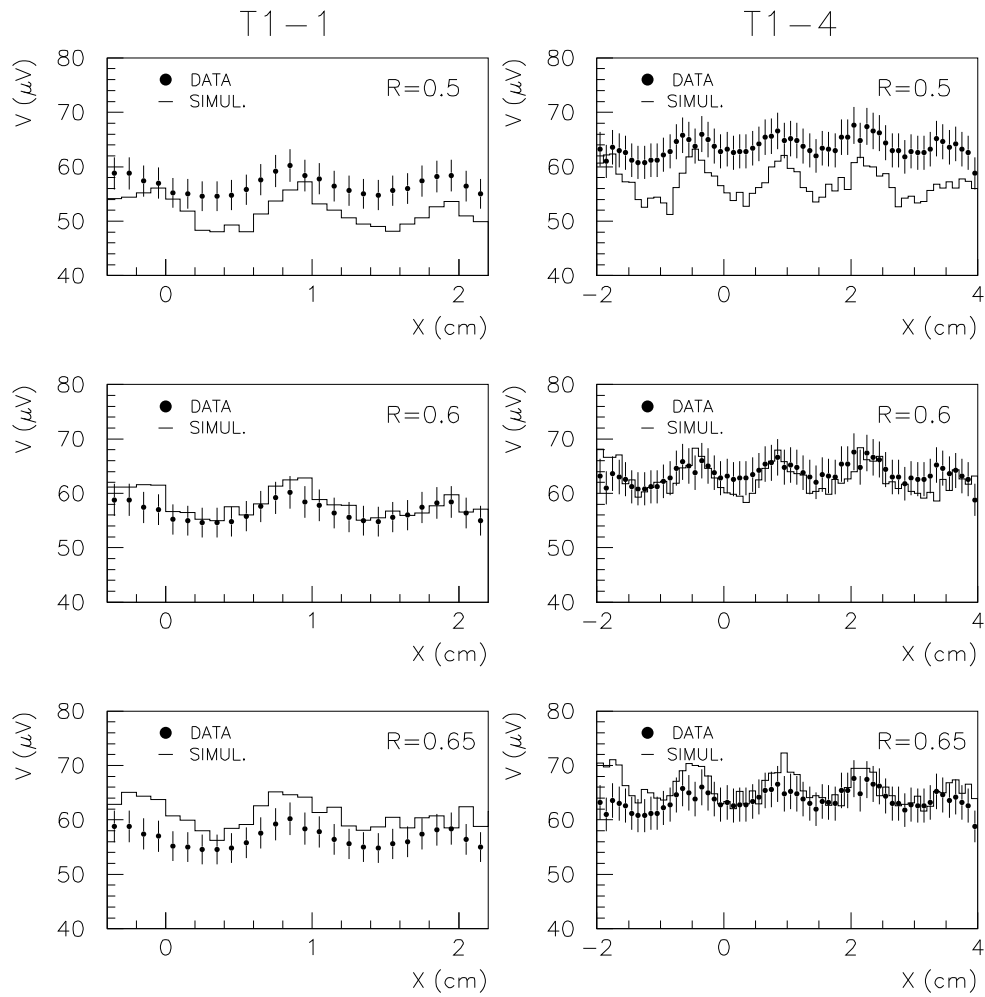


Figure 15: Comparison between data and Monte Carlo for a B1 type scan on tiles T1-1 and T1-4 wrapped with Tyvek paper for three different values of simulated effective reflection coefficient  $R$ .

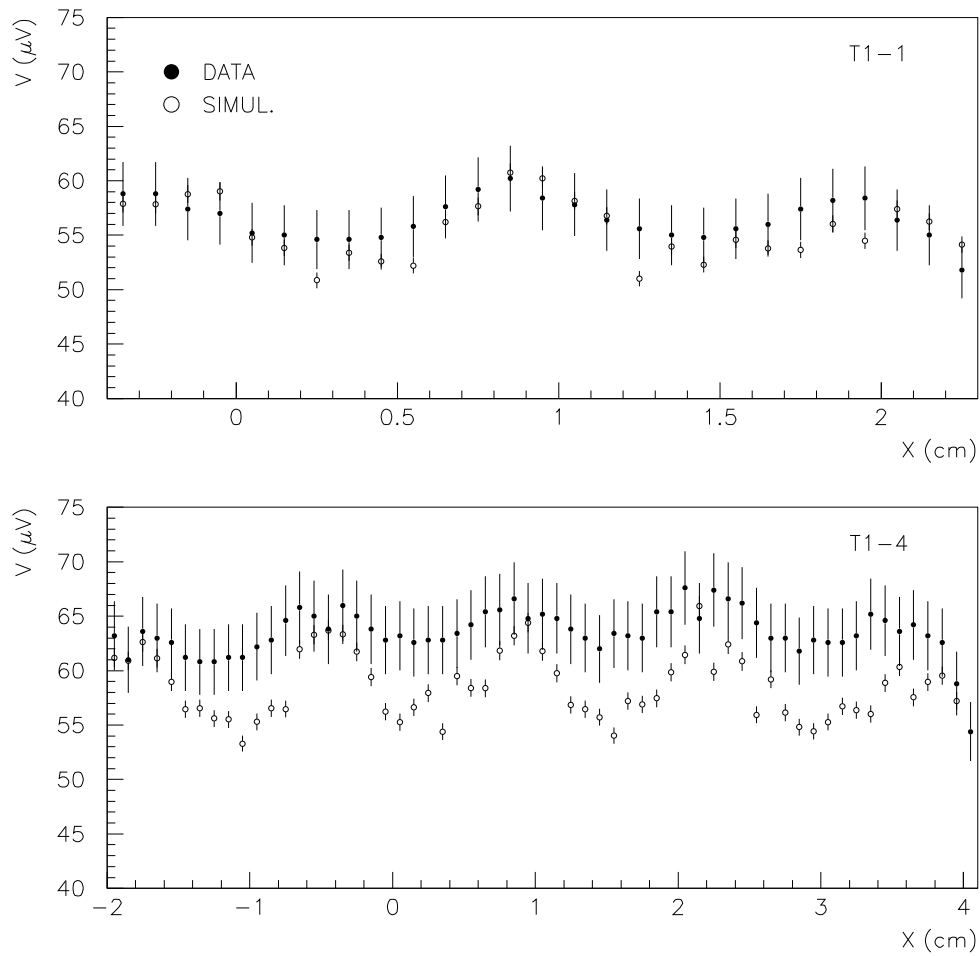


Figure 16: Comparison between data and Monte Carlo for a B1 type scan on tiles T1-1 and T1-4 wrapped with Tyvek paper for  $\lambda_{at} = 10$  cm,  $r_{fib} = 0.15$  and  $R = 0.6$ . While the data of the small tile T1-1 is well reproduced by the Monte Carlo, a good agreement between data and Monte Carlo is not obtained for the bigger tile T1-4.

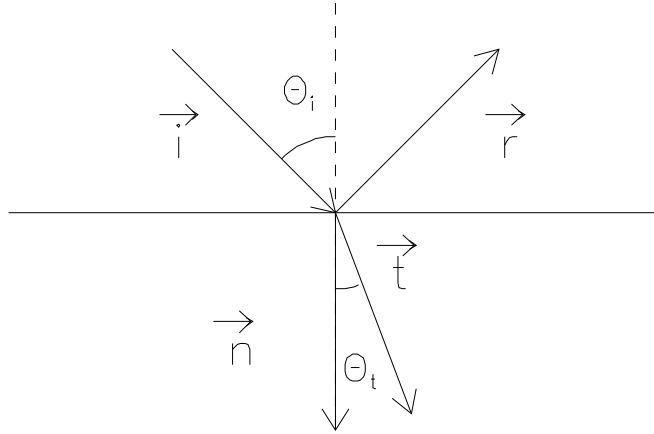


Figure 17: The definition of the normalized vectors  $\vec{i}$ ,  $\vec{r}$ ,  $\vec{t}$  and  $\vec{n}$  for incident, reflected and transmitted photons and the normal to the separation surface, respectively.